Advanced Characterisation of Pavement and Soil Engineering Materials – Loizos, Scarpas & Al-Qadi (eds)
© 2007 Taylor & Francis Group, London, ISBN 978-0-415-44882-6

Modeling test rolling on cohesive subgrades

J.P. Hambleton & A. Drescher
Department of Civil Engineering, University of Minnesota, Minneapolis, MN, USA

ABSTRACT: Test rolling is a quality assessment technique performed on road construction materials to verify consistency prior to paving. In this test, the depth to which the wheels of a heavy vehicle penetrate the material is used as a measure of quality. Current test rolling specifications are based largely on empirical data. In this paper, theoretical models are presented for the case of a test roller on cohesive soil which may be used to evaluate the effects of soil properties, wheel geometry, and wheel load on wheel penetration depth. The case of a towed wheel is considered. An approximate analytic approach premised on a three-dimensional bearing capacity formulation is presented for indentation and steady-state rolling of rigid wheels. The finite element code ABAQUS is used to perform three-dimensional simulation and validate the analytic approach. Theoretical predictions are compared to experimental data, and reasonable agreement is found.

1 INTRODUCTION

In test rolling procedures typically used in road construction practice, a towed or self-propelled vehicle is operated on subgrade or base materials after placement, and the vertical penetration depth or the depth of the permanent rut behind the wheels is recorded. Soil consistency is considered satisfactory if the penetration (and/or rut depth) is smaller than a specified limit, and reworking of the soil is required when the penetration is larger. The large areas that may be inspected and the ease with which severe problem areas are identified are the advantages of test rolling over other verification procedures. The test rolling process, however, is not well understood, and acceptance criteria are either empirically formulated or left simply to the discretion of project inspectors.

With a view towards refining the understanding of test rolling, this paper focuses on theoretical prediction of load-penetration relationships for indentation and steady-state rolling of rigid, right-cylindrical wheels. Indentation is considered due to its relevance in the initial stages of soil failure and as a basis for extension and comparison to the rolling case. In both indentation and rolling, the process is considered quasi-static, and in the rolling case, only towed wheels are considered, in which no torque is transmitted to the wheel about the point of rotation. Purely cohesive materials are addressed in this paper, although the analytic and numerical models can be readily extended to incorporate frictional soil behavior.

2 ANALYTIC APPROACH

2.1 *Bearing capacity theory*

The analytic approach presented in this paper is based on the concept of bearing capacity of shallow foundations and the formula widely used in geotechnical practice. Bearing capacity is identified as the average ultimate stress q_u acting at the foundation-soil interface when the soil fails plastically. Based on the work of Terzaghi (1943) and Meyerhof (1963), the generalized formula

for bearing capacity, which accounts for foundation shape and depth, has the following form (cf. Das 2005):

$$q_u = cN_c F_{cs} F_{cd} + qN_q F_{qs} F_{qd} + 0.5\gamma BN_\gamma F_{\gamma s} F_{\gamma d} \tag{1}$$

where c is soil cohesion; γ is soil unit weight; B is the smaller dimension of a rectangular footing; and q is the surcharge (pressure) on the soil acting at the depth D of the footing, given by $q = \gamma D$.

In Equation (1), N_c, N_q, and N_γ are the bearing capacity factors solely dependent on the soil friction angle φ, and F_{cs},… and F_{qd},… are the shape and depth factors. These factors were derived from theoretical considerations and empirical data, and various forms have been presented in the literature. In this paper, the factors listed by Das (2005) are applied. Considering purely cohesive material ($\varphi = 0$), the resulting formula for q_u is

$$q_u = 5.14c\left(1 + 0.19\frac{B}{L}\right)\left(1 + 0.4\frac{D}{B}\right) + \gamma D \tag{2}$$

where L is the longer dimension of a rectangular footing. In the test rolling problem, the total force Q rather than average stress q_u is of interest, and the former is calculated as $Q = q_u$BL.

The concept of bearing capacity applies to a rigid footing of fixed contact dimensions and depth. It is now postulated that indentation – and similarly rolling – can be understood as a sequence of yielding states each requiring average ultimate bearing capacity q_u, which can be computed using Equation (2) by appropriately selecting the contact dimensions and depth. In contrast to the notion of predicting load at incipient failure, the end result of the analytic method is prediction of load-penetration relationships. Unlike foundations, the contact region between the wheel and soil is not flat. However, if the penetration of the wheel is small in relation to wheelís diameter, considering the contact area of the wheel as a flat surface seems fully warranted.

2.2 *Indentation*

The concept of a fully rigid wheel has been employed extensively by researchers interested in soil-wheel interaction (cf. Karafiath & Nowatski 1978) and applies to the case where the wheel is very stiff relative to the soil. Figure 1 illustrates indentation of a rigid, right-cylindrical wheel and the relevant geometric parameters: sinkage (penetration) s, wheel diameter d, wheel width b, contact length h, and contact angle α. The term *sinkage* is used for consistence with previous work on vehicle-terrain interaction and refers always to the distance between the lowermost part of the wheel and the undisturbed soil surface.

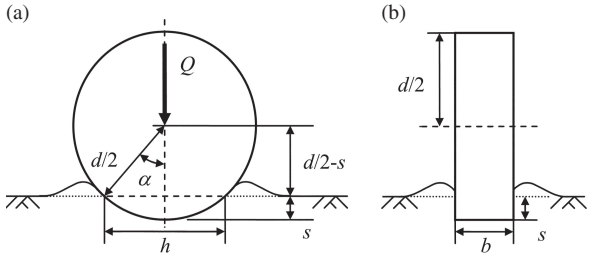

Figure 1. Schematic of indentation with rigid, right-cylindrical wheel: (a) cross section in plane of wheel diameter; (b) cross section in plane of wheel width.

When the wheel indents the soil, it displaces a certain amount of material outside the contact area (Fig. 1). Any displaced material is neglected in determining the contact area, because the exact configuration of the deformed soil is unknown. Therefore, the contact length h is given by

$$h = 2\sqrt{ds - s^2} \tag{3}$$

and the equivalent footing lengths B and L in Equation (2) are

$$\left.\begin{matrix} B = h \\ L = b \end{matrix}\right\} \text{ for } h < b \text{ , } \left.\begin{matrix} B = b \\ L = h \end{matrix}\right\} \text{ for } h \geq b \tag{4}$$

Although it is not considered in computing h, the resistance added by the upheaved material is accounted for through the equivalent footing depth D, which is assumed to depend only on the displaced material. For a fully-saturated (incompressible) clay-type material, the volume of material occupied by the wheel equals the volume displaced upwards. Considering one half of the wheel, the volume of soil displaced by the wheel V_d is

$$V_d = \frac{1}{8}bd^2\alpha - \frac{1}{4}bh\left(\frac{d}{2} - s\right) = \frac{1}{8}bd^2\cos^{-1}\left(1 - 2\frac{s}{d}\right) - \frac{1}{4}bh\left(\frac{d}{2} - s\right) \tag{5}$$

With regard to the bearing capacity plasticity solution considered by Prandtl (1921), the displaced volume can be approximated by a set of rectangular prisms with dimensions governed by b, h, and D, and the volume of soil displaced upwards V_u can be approximated as

$$V_u = 2bhD \tag{6}$$

Setting $V_d = V_u$ and keeping only the linear term in a series expansion about $s = 0$ gives

$$D = \frac{1}{6}s \tag{7}$$

Using the bearing capacity formula (2) together with the equivalent foundation parameters from Equations (3), (4), and (7) gives an explicit expression for the wheel force

$$Q = 2b\sqrt{ds - s^2}\left[5.14c\left(1 + 0.39\frac{\sqrt{ds - s^2}}{b}\right)\left(1 + 0.03\frac{s}{\sqrt{ds - s^2}}\right) + 0.17\gamma s\right] \tag{8}$$

for $h \leqslant b$ and

$$Q = 2b\sqrt{ds - s^2}\left[5.14c\left(1 + 0.1\frac{b}{\sqrt{ds - s^2}}\right)\left(1 + 0.07\frac{s}{b}\right) + 0.17\gamma s\right] \tag{9}$$

for $h > b$. In Equations (8) and (9), the unit weight contributes insignificantly to Q and can therefore be neglected.

2.3 *Steady-state rolling*

For rolling (Fig. 2a), the relationship between force and sinkage for a steady state is assessed without regard for the transient process required to reach that state. Wheel rolling is different from wheel indentation in that the contact area is reduced and that the total force Q is no longer vertical but inclined at an angle β. In the present analysis employing the bearing capacity concept, the inclination of the average ultimate stress is unknown. The angle β is related to the distribution of the normal stress σ_n and shear stress σ_t acting on the wheel as a result of contact (Fig. 2a).

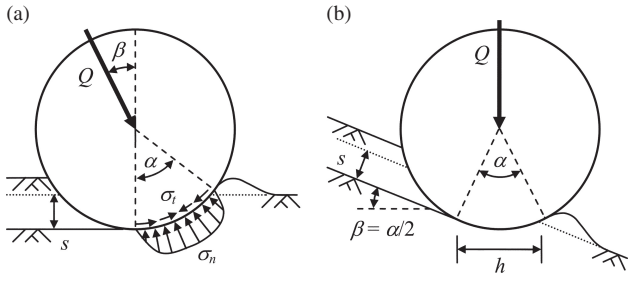

Figure 2. Schematic of rolling, rigid wheel in steady state: (a) deformed configuration and distribution of contact stresses; (b) steady-state rolling as shallow foundation on sloping ground.

Onafeko & Reece (1967) and Krick (1969) measured the normal and shear contact stresses on rigid wheels operating in agricultural soils. Their results suggest that one can reasonably approximate that the normal stresses are symmetrically distributed and shear stresses are antisymmetrically distributed about the bisecting angle $\alpha/2$, as illustrated in Figure 2a. With such symmetries, global equilibrium requires $\beta = \alpha/2$. It is therefore proposed that the angle β can be computed as

$$\beta = \frac{1}{2}\cos^{-1}\left(1 - 2\frac{s}{d}\right) \approx \sqrt{\frac{s}{d}} \tag{10}$$

and for $0 < s/d < 0.1$, $0 < \beta < 18°$. Using the data given by Onafeko & Reece, the actual values of β determined from direct measurements of the vertical and horizontal components of the wheel force agree with those predicted by Equation (10) to within -7 to 5%.

The generalized bearing capacity formula can account for non-vertical loading through inclination factors F_{ci}, F_{qi}, and $F_{\gamma i}$. It is therefore possible to use the same analysis considered for indentation (Section 2.2) except with a reduced contact area and $F_{ci}(\beta) \leqslant 1$. Alternatively, the rolling wheel problem may be considered analogous to the shallow foundation problem in which the load is perpendicular to the foundation but the foundation itself is inclined at the angle β (Fig. 2b). With this, the configuration has similarity to the ultimate bearing capacity problem for a shallow footing on sloping ground. The latter approach considering the footing to be inclined is used in this paper. With this, a small error arises due to the actual orientation of gravity and because, strictly speaking, $N_\gamma \neq 0$ in the unsymmetric problem.

Based on work by Hansen (1970) and Chen (1975), the bearing capacity formula for cohesive soil can be adapted to work for the case of sloping ground by using modified forms of the factors N_c and N_q. Little work has been done to determine shape and depth factors for the case of a footing on a slope, and in the present method the shape and depth factors for a horizontal footing are used, justified by the fact that β is small. The resulting formula for bearing capacity on sloping, cohesive soil, with the unit weight neglected, may be written as

$$q_u = 5.14c\left(1 + 0.19\frac{B}{L}\right)\left(1 + 0.4\frac{D}{B}\right)(1 - 0.39\beta) \tag{11}$$

Although the distribution of displaced soil may be different than in indentation, the same approximate expression (7) is used for D. Also, the contact length h is taken as the length of the chord subtending α, and

$$h = \sqrt{ds} \tag{12}$$

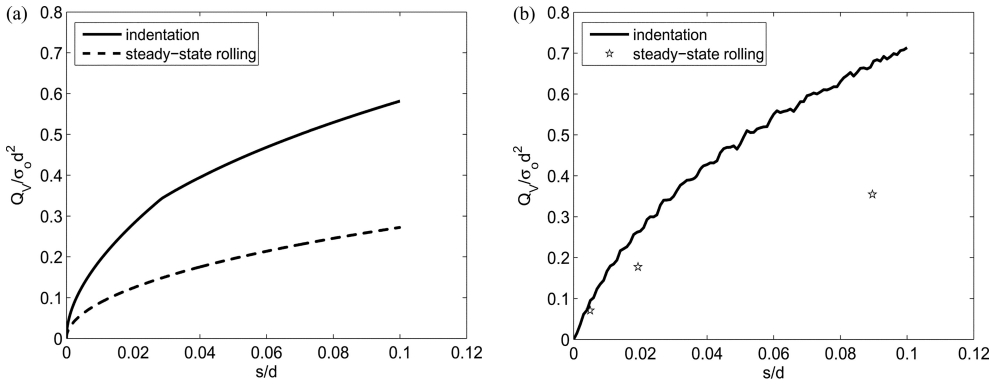

Figure 3. Vertical force versus sinkage: (a) analytic approach with $b/d = 0.33$; (b) ABAQUS simulations with $b/d = 0.33$, $E/\sigma_o = 250$, $\nu = 0.45$, $\mu = 0.85$, and $(\sigma_t)max = \sigma_o/2$.

The equivalent foundation lengths B and L are again given by Equation (4). The resulting formula for the total wheel force is

$$Q = 5.14bc\sqrt{ds}\left(1+0.19\frac{\sqrt{ds}}{b}\right)\left(1+0.07\sqrt{\frac{s}{d}}\right)\left(1-0.39\sqrt{\frac{s}{d}}\right) \tag{13}$$

for $h \leqslant b$ and

$$Q = 5.14bc\sqrt{ds}\left(1+0.1\frac{b}{\sqrt{ds}}\right)\left(1+0.07\frac{s}{b}\right)\left(1-0.39\sqrt{\frac{s}{d}}\right) \tag{14}$$

for $h > b$. The total force can be decomposed into its vertical and horizontal components using $Q_V = Q\cos\beta$ and $Q_H = Q\sin\beta$, respectively.

Figure 3 illustrates the relationship between the vertical force and sinkage for indentation and rolling using Equations (8) & (9) and Equations (13) & (14), respectively. In both cases, the response curve is characteristically concave downwards. For a given sinkage, the vertical force in rolling is roughly one-half of that in indentation.

3 NUMERICAL SIMULATIONS

Quasi-static indentation and rolling analyses were performed using the three-dimensional finite element software ABAQUS/Explicit, which is a dynamic code employing an explicit solution scheme (*ABAQUS* 2004). This code was chosen both for its computational efficiency in solving contact problems with large, plastic deformations and for its adaptive meshing capability. Mid-analysis remeshing is a virtual requisite for simulation of the rolling process due to the severe element distortions that result otherwise. The analysis of a rolling, rigid wheel bears similarity to that performed by Chiroux et al. (2005).

3.1 *Material model*

The soil in the numerical simulations was isotropic and elastoplastic, with linear elasticity and rate-independent, perfect plasticity. Because of inherent difficulties in implementing numerically

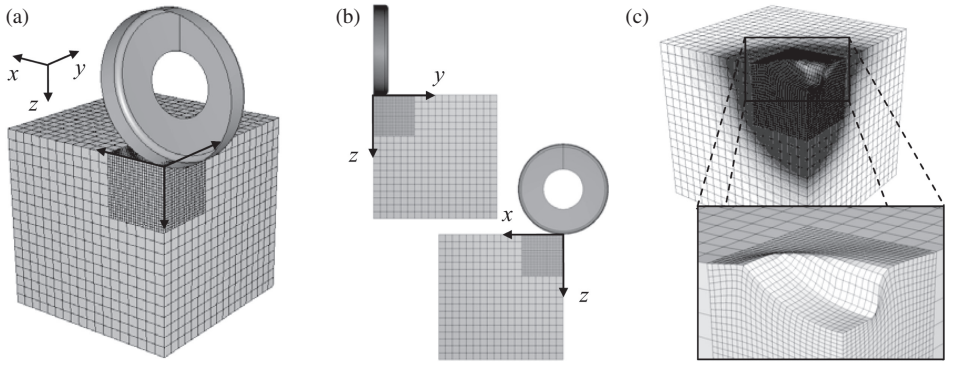

Figure 4. ABAQUS simulation of indentation with rigid wheel: (a) isometric view of reference configuration; (b) reference configuration in *y*-*z* plane and *x*-*z* plane; (c) contours of generalized shear stress (darker implies higher intensity) and deformed soil configuration (wheel not shown for clarity).

the Tresca yield condition (tacitly assumed in the analytic approach), the soil was modeled using the closely-related von Mises yield condition

$$(\sigma_1 - \sigma_2)^2 + (\sigma_2 - \sigma_3)^2 + (\sigma_3 - \sigma_1)^2 = 2\sigma_o^2 \tag{15}$$

where σ_1, σ_2, and σ_3 are principal stresses and σ_o is the material yield strength in uniaxial tension or compression. The left-hand side of Equation (15) is a stress invariant referred to in this paper as *generalized shear stress*. Using $\sigma_o = 2c$ or $\sigma_o \approx 1.73c$, the von Mises yield surface circumscribes or inscribes, respectively, the Tresca yield surface in principal stress space. Plastic deformation was prescribed according to the associated flow rule, which was integrated using the backward Euler method in the incremental plasticity formulation. Like the Tresca yield condition used in the analytic approach, the von Mises yield condition with the associated flow rule gives pressure-independent (purely cohesive) and incompressible plastic behavior.

3.2 *Indentation*

The reference configuration used in ABAQUS for three-dimensional analysis of rigid wheel indentation is shown in Figure 4. There are two planes of symmetry for the indentation problem, one in the *x*-*z* plane and one in the *y*-*z* plane, so that only one quarter of the domain of the full problem was simulated. One half of the wheel is shown, but only one quarter participated in the simulation.

The wheel was simulated using an analytical rigid shell, where *analytical* in this case means that it is not discretized. The interior of the shell is visible in the isometric view of Figure 4a. The wheel is right-cylindrical with an edge fillet of radius r_f. A non-zero fillet radius is required to avoid numerical problems arising in the algorithm used to model contact between the wheel and the soil. Since the wheel is rigid, boundary conditions are conveniently prescribed on a single reference point which governs the response of the entire body. Realistic mass and rotational inertia were assigned at the reference point, located at the wheel center.

The soil was discretized using linear, 8-node, reduced integration, hexahedral elements. The soil was partitioned into two regions of different element sizes (Fig. 4) to accommodate the large displacement gradients occurring near the wheel. The two regions were connected using the tie constraint available in ABAQUS for rapid mesh transition.

The exact mesh configuration depended on the specific wheel geometry and material properties. For $b/d = 0.3$, a maximum sinkage of $s/d = 0.1$, and typical material parameters, the overall soil domain was taken as a cube with edge length roughly $1.5d$, and the region of small elements

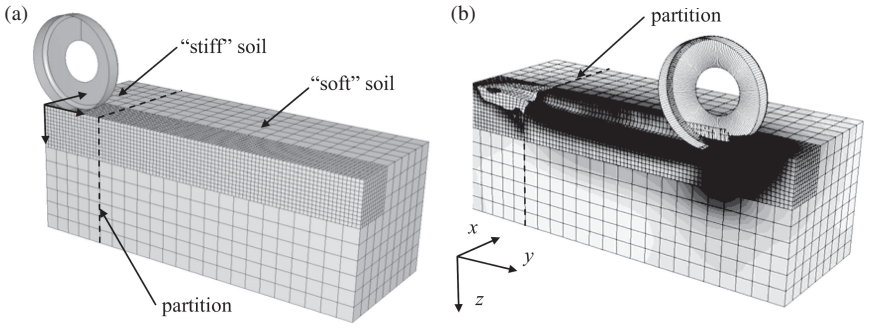

Figure 5. ABAQUS simulation of rolling rigid wheel: (a) reference configuration; (b) contours of generalized shear stress (darker implies higher intensity) and deformed soil configuration at end of rolling simulation.

was taken as a cube with length 0.5d. The elements in the model were nearly cubic, which was a desirable aspect of the mesh grading used. The larger elements had an edge length of approximately 0.08d, and the smaller elements had length 0.02d. The total number of elements was roughly 20,000. The simulation results were practically unaffected by refining the mesh further or increasing the size of the soil domain (Hambleton 2006).

Symmetry boundary conditions were applied to the soil in the x-z and y-z planes by enforcing zero nodal displacements in the y- and x-directions, respectively. The soil face in the x-y plane was traction-free, except where tractions developed as a result of contact. Contact between the wheel and soil was governed by either a classical Coulomb friction rule or a "rough" contact model in which no slip was permitted between points in contact. For simplicity, a single coefficient of friction μ was used in the former for both sticking and sliding contact, with a maximum shear stress $(\sigma_t)_{max}$ also governing the onset of slip. On the soil faces not visible in Figure 4a, out-of-plane displacements were fixed, but the soil was free to displace in the remaining two degrees of freedom.

To introduce the unit weight of the soil, a uniform body force was first applied to the soil in the z-direction. Next, the wheel was displaced into the soil in the z-direction at a constant velocity. Step times and velocities were chosen to minimize dynamic effects in the model, while keeping computation time reasonable. The adaptive meshing algorithm available in ABAQUS was used while the wheel was being indented to preserve the aspect ratio of the elements.

Example simulation output is shown in Figures 3b and 4c. Note that the shape of the force-sinkage curve from the simulation (Fig. 3b) qualitatively matches the force-sinkage curve predicted using the analytic method (Fig. 3a).

3.3 *Rolling*

The reference configuration used for rigid wheel rolling is shown in Figure 5a. The y-z plane, the midplane of the full wheel, is the only plane of symmetry in the rolling problem, allowing for one half of the full problem to be simulated as depicted. The rigid wheel used in the rolling case is identical to that used for indentation. The wheel in Figure 5a is oriented relative the reader as in Figure 3a for indentation and rolls in the y-direction during the simulation.

During the test rolling process, the test roller typically rolls from a region of stiff soil in which very little penetration occurs into a region of soft soil in which it penetrates more readily. To simulate this, the soil was partitioned into a stiff region and a soft region as shown in Figure 5a. In this context, the relative "stiffness" or "softness" of the soils may involve elastic properties, plastic properties, or both, but in any case, the wheel penetrates farther into the soft material than the stiff material.

Again, the soil discretization consisted of two regions of different element sizes connected through the tie constraint, using the same element type as with indentation. In the x-z plane, the overall soil domain was a square with edge length roughly 1.5d for typical parameters, with the

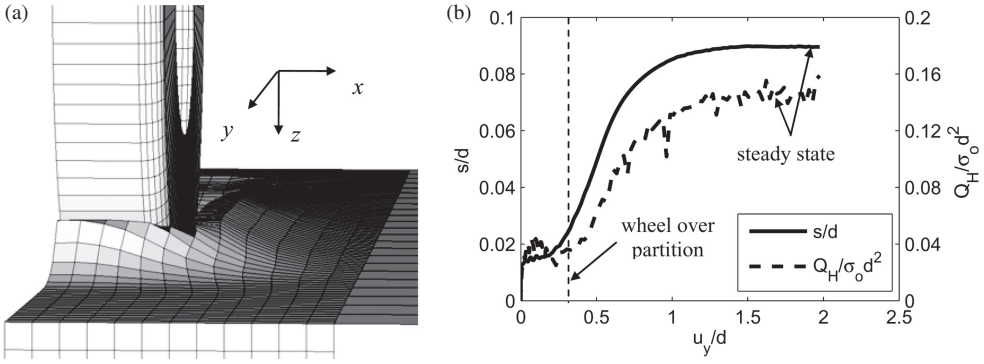

Figure 6. Output from ABAQUS simulation of rolling wheel: (a) view of deformed region; (b) sinkage and horizontal wheel force versus horizontal wheel displacement.

region of smaller elements taken as a square with length $0.5d$. The length of the soil region parallel to the y-axis was roughly $3.5d$. The interface between the stiff and soft soil was at $y \approx 0.75d$, and the wheel was initially located at $y \approx 0.4d$. Since the rolling process occurs over a longer period than indentation and smaller time increments are needed for computational stability due to greater element distortion, a coarser mesh than used for indentation was implemented. For a typical wheel, the larger elements had an edge length of approximately $0.16d$, and the smaller elements had length $0.04d$. The total number of elements was therefore about 15,000.

All displacements and rotations of the wheel were fixed except displacements in the y- and z-directions and rotation about the x-direction, so that the wheel could displace into the soil, move forward, and rotate freely. Free rotation is an essential part of simulating the towed condition, in which no torque (about the x-direction) is transmitted between the wheel and axle. The wheel rotates as a natural consequence of its frictional interaction with the soil. Friction at the interface between the wheel and soil was defined as discussed in Section 3.2.

During the simulation, a uniform body force representing unit weight was first applied to the soil. Next, a concentrated force Q_V (acting in the z-direction) was applied to the wheel and kept constant to simulate the axle load introduced by the weight of the test roller. After Q_V was applied, the wheel was given a linear velocity in the y-direction, ramping smoothly from zero velocity to a constant value. The wheel reached a constant linear velocity just before the wheel entered the region of soft soil. In the fourth and final stage of simulation, the wheel continued to roll forward at a constant linear velocity through the soft soil. As for indentation, loading rates were chosen such that inertial effects were negligible, and adaptive meshing was used to correct element distortions.

The deformed configuration at the end of a rolling wheel simulation is shown in Figure 5b. Figure 6a shows the deformed soil region near the wheel and reveals the need for three-dimensional analysis. In the three-dimensional simulation, material "flows" around the wheel, whereas material would continually accumulate in front of the wheel in an analogous two-dimensional analysis. Figure 5b gives the sinkage and horizontal wheel force as functions of horizontal wheel displacement u_y, showing both the transient and steady-state regimes. A single simulation gave one point on the force-sinkage curve for steady-state rolling, such that several simulations were needed to obtain the overall trend of the curve. Figure 3b gives an example of the resulting force-sinkage data. As with indentation, the resulting curve for steady-state rolling qualitatively matches the analytic curve (Fig. 3a).

4 EXPERIMENTS

An indentation experiment was conducted in the laboratory using a solid aluminum wheel with $d = 76$ mm and $b = 25$ mm and a saturated clay soil. The wheel was roughened by adhering

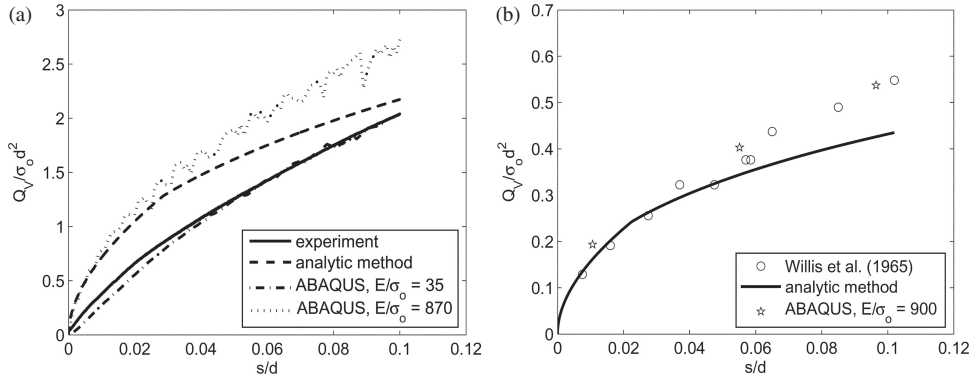

Figure 7. Comparison of theoretical predictions and experiments: (a) indentation; (b) steady-state rolling.

sandpaper to the contacting surface. After the clay was compacted and smoothed in a bin with length, width, and depth of 300, 240, and 100 mm, respectively, the wheel was indented at a constant velocity in the middle of the bin using a standard load frame. Force and displacement data were recorded using a load cell and displacement transducer. Unconfined compression tests were carried out on extracted specimens to determine the uniaxial yield strength σ_o of the material. The mean yield strength of the material was determined to be $\sigma_o = 57.7$ kPa. Based on triaxial tests, the clay was determined to have internal friction, with $\varphi \approx 3°$. The low friction angle warrants the assumption of pressure-independence.

Willis et al. (1965) obtained experimental data for several towed, rigid wheels operating in clay. They measured wheel sinkage under varying values of vertical wheel force, presumably under steady conditions. Their results for a rigid wheel with $d = 508$ mm, $b = 76$ mm, and a clay with cohesion $c = 30$ kPa are given in Figure 7b. The clay had a reported friction angle of 7°.

5 COMPARISON OF RESULTS

Figure 7 compares the predictions from the analytic method and the numerical simulations with the results from the experiments discussed in Section 4. For indentation, two simulations were run to evaluate the effect of soil elasticity. In the first, the Youngís modulus $E = 2$ MPa was that determined approximately from the unconfined compression tests, and a Poissonís ratio of 0.45 was assumed. In the second, $E = 50$ MPa was sufficiently large to make elastic deformation negligible. The "rough" contact model was used for the indentation simulations, and the fillet radius of the wheel was taken as $r_f = b/12$. For the analytic prediction, the cohesion was taken as $c = \sigma_o/1.87$ to match the von Mises yield condition used in ABAQUS. A unit weight of 20 kN/m^3 was assumed, though the presence of unit weight in the simulations was practically unimportant.

For the numerical simulations of rolling, the contact properties were $\mu = 0.8$ and $(\sigma_t)_{max} = c$, although these parameters were not considered by Willis et al. (1965). Since they were also not reported, additional parameters were specified as for indentation, with a large elastic modulus to eliminate appreciable elastic deformation.

It is evident in Figure 7 that the experimental data exhibits the same trends as predicted theoretically from the analytic method and numerical simulations. With appropriate choice of elastic modulus, the numerical simulations are capable of giving a very accurate prediction of the experimental force-sinkage curves. More surprising is that the predictions using the analytic method are fairly close to the experimental data. Output from the numerical simulations using large elastic moduli agrees rather well with the curves from the analytic approach, especially at small sinkage.

6 CONCLUSIONS

The agreement between theoretical predictions and experiments (Fig. 7) offers compelling evidence that both the approximate analytic approach and the numerical simulations yield fairly accurate predictions. The appeal of the analytic method is that it offers a closed-form prediction. The numerical simulations are more flexible in that they can accommodate elasticity and other effects, though they are comparatively time-consuming and capable of giving only case-wise results.

Although this paper concerns only cohesive soil, the approaches presented may be extended to frictional soil. It should be evident that the analytic approach can be developed with $\varphi \neq 0$ and that a pressure-dependent yield condition can be implemented in the numerical simulations to investigate granular materials. Wheel flexibility and non-right-cylindrical wheel geometries can also be introduced in the approximate analytic approach and numerical simulations, as demonstrated by Hambleton (2006).

The theoretical analyses discussed in this paper make possible greater sophistication in the interpretation of test rolling results and may be used to develop more advanced test rolling techniques than those currently practiced. The penetration depth (sinkage) of a test roller is an especially easy measurement to obtain in the field, and an ultimate goal of analyzing the test rolling process is to ascertain how soil properties can be deduced from this depth. For example, the analytic approach presented in Section 2, which applies to a purely cohesive soil with negligible elasticity, suggests that there is a unique relationship between penetration depth and soil cohesion for a given wheel force and geometry. Test rolling, in this sense, is conceptually similar to the metal hardness tests, in which the penetration depth of an indenter is used to determine the tensile strength of the material.

ACKNOWLEDGEMENTS

The financial support provided by the Minnesota Local Road Research Board and the computer resources provided by the University of Minnesota Supercomputing Institute are gratefully acknowledged. Cooperation from the Minnesota Department of Transportation is greatly appreciated. The second author also acknowledges partial support from the Shimizu Corporation.

REFERENCES

ABAQUS Version 6.5 Documentation. 2004. Providence: ABAQUS, Inc.

Chen, W.F. 1975. *Limit Analysis and Soil Plasticity*. Amsterdam: Elsevier.

Chiroux, R.C., Foster Jr., W.A., Johnson, C.E., Shoop, S.A. & Raper, R.L. 2005. Three-dimensional finite element analysis of soil interaction with a rigid wheel. *Applied Mathematics and Computation* 162(2): 707–722.

Das, B.M. 2005. *Fundamentals of Geotechnical Engineering*. Toronto: Thomson.

Hambleton, J.P. 2006. *Modeling Test Rolling*. Masterís Thesis. Minneapolis: University of Minnesota.

Hansen, J.B. 1970. *A revised and extended formula for bearing capacity*. Bulletin 28. Copenhagen: Danish Geotechnical Institute.

Karafiath, L.L. & Nowatzki, E.A. 1978. *Soil Mechanics for Off-Road Vehicle Engineering*. Clausthal: Trans Tech.

Krick, G. 1969. Radial and shear stress distribution under rigid wheels and pneumatic tires operating on yielding soils with consideration of tire deformation. *Journal of Terramechanics* 6(3): 73–98.

Meyerhof, G.G. 1963. Some recent research on bearing capacity of foundations. *Canadian Geotechnical Journal* 1(1): 16–26.

Onafeko, O. & Reece, A.R. 1967. Soil stresses and deformations beneath rigid wheels. *Journal of Terramechanics* 4(1): 59–80.

Prandtl, L. 1921. Über die Eindringungs-festigkeit (Härte) plastischer Baustoffe und die Festigkeit von Schneiden. *Zeitschrift für Angewandte Mathematik und Mechanik* 1(1): 15–20.

Terzaghi, K. 1943. *Theoretical Soil Mechanics*. New York: Wiley.

Willis, B.M.D., Barret, F.M. & Shaw, G.J. 1965. An investigation into rolling resistance theories for towed rigid wheels. *Journal of Terramechanics* 2(1): 24–53.